Journal of Power Sources 195 (2010) 7129–7139

Contents lists available at ScienceDirect

Journal of Power Sources

journal homepage: www.elsevier.com/locate/jpowsour

Review

Seal glass for solid oxide fuel cells

M.K. Mahapatra, K. Lu*

Department of Materials Science and Engineering, Virginia Polytechnic Institute and State University, Blacksburg, VA 24061, USA

ARTICLE INFO

Article history:
Received 16 April 2010
Received in revised form 31 May 2010
Accepted 1 June 2010
Available online 8 June 2010

Keywords:
Solid oxide fuel cell
Seal glass
Thermal stability
Devitrification resistance
Thermomechanical property
Electrical resistivity

ABSTRACT

Seal glass plays a crucial role in solid oxide fuel cell performance and durability. In this review paper, overall composition–structure–property relations of seal glasses are discussed from bulk glass behavior, interfacial interaction, and sealing ability point of view. A seal glass should have a combination of desired thermal, chemical, mechanical, and electrical properties in order to seal cell components and stacks and prevent gas leakage. It must be stable for ~40,000 h at 500–1000 °C in oxidizing and reducing atmospheres and withstand ~10,000 thermal cycles between room temperature and cell operating temperature. A $SrO–La_2O_3–Al_2O_3–SiO_2$ based seal glass shows the promise to meet all the desired thermophysical properties, long-term stability, and thermal cycling resistance. In this paper, the most recent advances in the field are discussed along with this glass. Future seal glass research directions for solid oxide fuel cells are also analyzed.

Contents

1. Introduction

Energy demand is increasing exponentially with continued growth of world population, economy, and living standards. Limited reserve of fossil fuel and emission of greenhouse gases (CO_x, NO_x, SO_x) from its use are threatening the present and future generations in terms of energy crisis, environmental pollution, global warming, and health hazards. Sustainable energy is much needed in order to address these problems.

Fuel cells are attractive electrochemical devices that convert hydrogen or hydrocarbon into electricity without any moving parts during operation. When hydrogen is used as a fuel, water is the by-product. Example fuel cells are phosphoric acid fuel cell, proton exchange membrane fuel cell, molten carbonate fuel cell, solid oxide fuel cell, and alkaline fuel cell. Among these differ-

* Corresponding author. Tel.: +1 540 231 3225; fax: +1 540 231 8919.
E-mail addresses: mkmanoj@vt.edu (M.K. Mahapatra), klu@vt.edu (K. Lu).

0378-7753/$ – see front matter © 2010 Elsevier B.V. All rights reserved.
doi:10.1016/j.jpowsour.2010.06.003

Table 1
State-of-the-art materials for SOFCs [3–5].

Components	High temperature SOFC (900–1000 °C)	Intermediate temperature SOFC (700–900 °C)	Low temperature SOFC (500–700 °C)
Anode	Nickel/fully stabilized zirconia cermet	Nickel/fully stabilized zirconia cermet	Nickel/fully stabilized zirconia cermet
Cathode	Strontium-doped lanthanum manganate (LSM), LSM-fully stabilized zirconia composite	Strontium-doped lanthanum manganate (LSM), LSM-fully stabilized zirconia composite	Strontium-doped lanthanum cobaltite, Strontium-doped lanthanum cobaltite ferrite
Electrolyte	Scandia, yttria, or ceria fully stabilized zirconia	Scandia, yttria, or ceria fully stabilized zirconia	Gadolinia-doped ceria
Interconnect	Doped lanthanum chromite	Chromia based ferritic stainless steel	Chromia based ferritic stainless steel

ent fuel cells, solid oxide fuel cells (SOFCs) are the most preferred due to their higher efficiency, fuel flexibility, and cost effectiveness. However, SOFCs have to be operated at high temperatures (500–1000 °C) to realize these advantages. When a SOFC is operated in the reverse mode, it is called solid oxide electrolyzer cell and can generate hydrogen by splitting water. In this paper, we will focus the discussion on SOFCs with the understanding that most knowledge can be directly applied to solid oxide electrolyzer cells.

SOFC operates based on Nernst equation to generate electrical voltage (E) from oxygen partial pressure difference at the electrodes:

$$E = \left(\frac{RT}{4F}\right) \ln\left(\frac{P_{O_2(C)}}{P_{O_2(a)}}\right) \quad (1)$$

where R is the gas constant, T the temperature, F the Faraday constant, and $P_{O_2(C)}$ and $P_{O_2(a)}$ are the partial pressures of oxygen at the cathode and the anode, respectively. A SOFC mainly consists of electrodes (anode and cathode), electrolyte, and interconnect. Oxygen gas from air is ionized to oxygen ions on the cathode side. The oxygen ions then migrate to the anode side through the electrolyte and combine with the fuel on the anode side. The interconnect collects current and provides integrity to the cell stacks.

SOFCs have great potentials for stationary and mobile applications such as residential, power grid, military, long duration mobile devices, and remote communication electronics. Energy conversion efficiency for SOFCs increases with operating temperatures and 56% has been achieved [1]. By cogeneration of heat and power, 65–85% efficiency can be achieved in a hybrid system [2]. SOFC can be classified into three types according to operating temperatures: high temperature SOFC (900–1000 °C), intermediate temperature SOFC (700–900 °C), and low temperature SOFC (500–700 °C). Typical SOFC operating temperature is ~800 °C. Most of the research has been carried out for intermediate temperature SOFCs. Reducing the operating temperature to 500–600 °C requires new electrolytes with high oxygen ionic conductivity, active catalysts for oxidation at the anode and reduction at the cathode, and electrode materials with suitable ionic and electronic conductivities. To produce electrical power in kilowatt to megawatt range, many cells need to be stacked through interconnect materials. The state-of-the-art materials for SOFC components are listed in Table 1.

There are mainly two designs for SOFCs: tubular and planar. Planar designs are preferred due to: (1) high power density, (2) a wide range of operating temperatures, (3) potential for both stationary and mobile applications, (4) design flexibility and ease of fabrication, and (5) lower cost [6]. For example, a current density of 0.3468 A cm^{-2} can be obtained from a planar design compared to 0.289 A cm^{-2} from a tubular design at the same operating condition [7]. This article will focus exclusively on the planar cell design. For this design, sealing is required along the edges of the cell components [6]. Example locations of seals in planar SOFCs are illustrated in Fig. 1. A seal material is a critical component of planar SOFCs because it seals the cells/stacks and prevents gas leakage and mixing. The efficiency of SOFCs degrades proportionally to the gas leakage rate because of decreased utilization of input fuels. Mixing of reducing and oxidizing gases also accelerates cell degradation and can even cause explosion [8,9].

There are three types of seals: compressive, compliant, and rigid. Mica and mica-based hybrid materials, metal-brazes, and glass/glass–ceramic materials are used as compressive, compliant, and rigid seals, respectively [6,10–12]. At cell operating temperatures, compressive seals require an applied load, which complicates cell design and increases fabrication cost. Compliant seals do not bond with the SOFC components well, are prone to oxidation and 'hydrogen embrittlement', and are electrically conductive. Rigid seals have many advantages compared to compressive and compliant seals. Glass and glass–ceramic seals rigidly bond to the cell components, can prevent leakage and mixing of gasses, and are electrically insulating. Additionally, glass and glass–ceramic seals are flexible in design, easy to fabricate, and cost-competitive [6,10–12]. A wide range of material properties required for sealing can be achieved with a glass or glass–ceramic seal by suitable compositional design.

Glass and glass–ceramics are the most preferred SOFC seal materials and the focus of this review paper. No distinction between glass and glass–ceramic seals will be made for

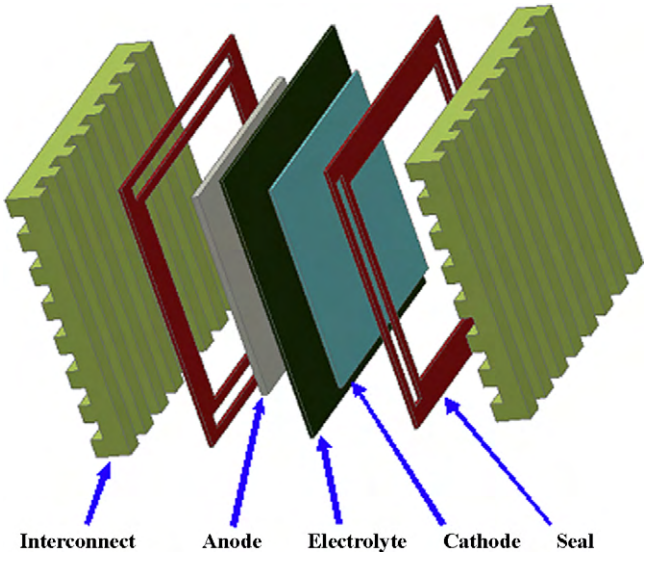

Fig. 1. Schematic of seal positions in a planar SOFC.

discussion convenience. The property requirements and compositional design challenges of seal glasses will be first explained. Composition–structure–property relations, interaction with interfacing components, and impact on SOFC performance and durability will be analyzed in detail. We have developed a $SrO–La_2O_3–Al_2O_3–SiO_2$ based seal glass which can fulfill all the sealing requirements. The guiding principles for this glass design will be provided. Finally, research needs and future directions in the SOFC sealing area will be discussed.

2. Requirements of seal glass in solid oxide fuel cells

Several physical and chemical properties and thermal stability should be obtained simultaneously in a seal material for proper SOFC operation. The most important physical properties include glass transition temperature (T_g), thermal expansion coefficient (CTE), and electrical resistivity. Chemical properties include resistance to chemical reaction with vapor gases and the resultant glass vaporization and degradation at cell operating temperatures (500–1000 °C) in oxidizing (cathode side) and wet reducing ($\geq$50 vol% H_2O, anode side) atmospheres. A seal material should be compatible with the interfacing components to avoid pores and cracks and gas leakage paths. Since SOFCs need to operate continuously for $\geq$5000 h for mobile applications and $\geq$40,000 h for stationary applications, and undergo thousands of thermal cycles between room temperature and operating temperature [13], a seal material should be stable and withstand thermal cycling without substantial property degradation for the entire period. Additionally, a seal glass should withstand thermal and mechanical stresses arising from material property differences, temperature gradient, and stack weight/external loads during operation and transportation. The electrical resistivity of a seal glass must be high enough to prevent SOFC from electrical shunting. Simultaneous fulfillment of these requirements is the main challenge in developing a suitable seal material [6,9–12].

3. Challenges in seal glass design

Seal glasses are multicomponent oxide systems which contain glass network formers, glass network modifiers, intermediates, and additives. Glass network formers are oxides of high field strength (1.0–2.0) and low coordination number (3–4) and provide polyhedral units in a glass network structure. Common network formers for seal glasses are SiO_2 and B_2O_3. Network modifiers are oxides of low field strength ($\leq$0.35) and high coordination number (8) [14,15]. They disrupt glass network structure, occupy random positions in-between the polyhedra, and maintain local charge neutrality [14,16]. Modifier oxides create non-bridging oxygen species which do not link the polyhedral units [14–16]. Common network modifiers are alkali oxides and alkaline earth oxides. Modifier oxides take the major role of modifying glass properties. Intermediate oxides have field strength (0.84–1.04) and coordination number (4–6) in-between those of the network formers and modifiers [14]. They can be either a glass former or a modifier depending on the specific glass composition. Al_2O_3 is the most commonly used intermediate oxide in seal glasses. Rare earth oxides (such as La_2O_3) and transition metal oxides (such as NiO, TiO_2, and ZnO) are often added into a seal glass to tailor the desired properties. These oxides are known as additives and can be either a network former or a network modifier depending on the specific glass composition [17].

Designs of seal glass compositions are mainly based on the knowledge of the field strength of the constituent cations and the 'additive rule'. Challenges arise due to three reasons: deviation of the 'additive rule' due to 'combined ion effect', 'boron anomaly', and lack of understanding of glass composition–structure–property relations. According to the 'additive rule', seal glass properties can be modified by varying constituents in a glass composition [14,16,18]. However, deviation of the 'additive rule' is frequently observed due to short-range interaction between different types of modifiers [16,18,19]. This phenomenon is known as 'combined ion effect'. From a different aspect, B_2O_3 is a common constituent in most of seal glass compositions. Modifier cations change glass properties anomalously by converting planar boroxyl structural groups to borate structural groups in B_2O_3-containing glasses. This phenomenon is known as 'boron anomaly'. The properties of a seal glass depend not only on the cationic field strength but also on the coordination number of cations, cation–oxygen bond length and bond angles, local ordering in the network structure, and the degree of network connectivity. Heterogeneity due to local ordering can occur at the atomic level in a multi-component seal glass [17,20–22].

4. Bulk seal glass properties

4.1. Thermal properties

There are four important thermal properties to consider for a SOFC seal glass: glass transition temperature (T_g), glass softening temperature (T_s), CTE, and devitrification resistance.

The glass transition temperature, T_g, is the temperature of the 'onset of glass transformation region' of a liquid to a frozen solid when the liquid is very rapidly cooled (quenched). The average viscosity of a glass at T_g is $10^{11.3}$ Pa s. Glass softening temperature, T_s, is the temperature at which a glass fiber of 24 cm long and 0.7 mm diameter elongates at the rate of 1 mm min^{-1} at the heating rate of 5 K min^{-1}. This is known as Littenton softening point and the viscosity of the glass at T_s is $10^{6.6}$ Pa s. For sealing glasses, the glass softening temperature is often determined from dilatometric studies and is the temperature at the maximum length of the glass sample on a length vs. temperature curve during heating. The viscosity of the glass at T_s is 10^8–10^9 Pa s [18]. In this context, T_g and T_s of a seal glass are important. The T_g value of a seal glass should be slightly below the cell operating temperature to relieve thermal stress and self-heal cracks [23,24]. For high temperature, intermediate temperature, and low temperature SOFC seal glasses, T_g should be in the temperature ranges of 750–850 °C, 650–750 °C, and 450–650 °C, respectively. T_s value should be higher than the cell operating temperature to avoid excessive glass flow. For high temperature, intermediate temperature, and low temperature SOFC seal glasses, T_s should be in the temperature ranges of 900–1000, 700–900, and 500–700 °C, respectively.

A seal glass generally contains 40–70 mol% network formers. T_g in 675–775 °C temperature range and T_s in 725–875 °C temperature range have been obtained for silicate glasses [25–31]. T_g and T_s generally increase with SiO_2 content because of a higher amount of bridging oxygen, higher network connectivity, and higher T_g and T_s of vitreous SiO_2. T_g in the 500–580 °C temperature range has been achieved for borate glasses [29–31]. Presence of planar boroxyl structural groups and low T_g of pure B_2O_3 (~275 °C) lead to low T_g for the B_2O_3-containing glasses [14,16]. For borosilicate glasses, T_g of 480–740 °C and T_s of 600–750 °C are obtained [28,32–42]. T_g and T_s decrease by 50–100 °C with the increase of B_2O_3/SiO_2 ratio as shown in Fig. 2 for borosilicate glasses [27,28,32,43]. The reasons are as follows [27,44]. First, both three-coordinated BO_3 and four-coordinated BO_4 structural units are present. An increase in the B_2O_3 content decreases the probability of silicon coordination with BO_4 units and results in less rigid network structure. Consequently, T_g and T_s decrease. Second, B_2O_3 addition increases the fraction of non-bridging oxygen containing borate and silicate structural units. The higher amount of non-bridging oxygen decreases network connectivity and thus T_g and T_s.

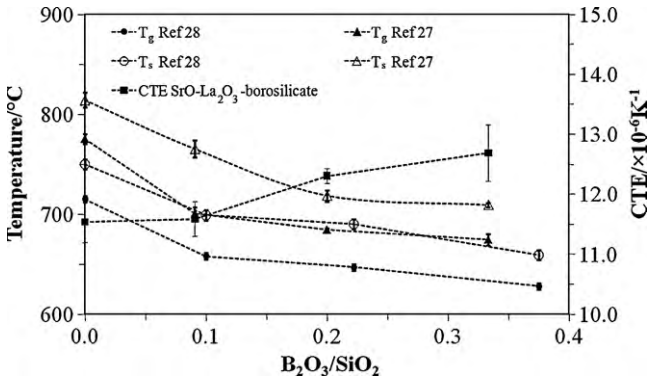

Fig. 2. Variation of T_g, T_s, and CTE as a function of B_2O_3/SiO_2 ratio in BaO–MgO–borosilicate and SrO–La_2O_3–borosilicate glasses [27,28].

A seal glass generally contains 20–45 mol% network modifiers. A wide range of T_g and T_s have been obtained in alkaline earth oxide-containing seal glasses. T_g of 500–675 °C and T_s of 650–750 °C are obtained in BaO-containing borosilicate glasses [25,28,34,36,38,39,41,43]. T_g of 625–775 °C and T_s of 700–825 °C are obtained in SrO–Al_2O_3–La_2O_3–B_2O_3–SiO_2 seal glass systems [27,32,33,35,37,42]. T_g of 610–720 °C is obtained for CaO-containing and MgO-containing borosilicate glasses [28,36,45]. Modifier oxides decrease T_g and T_s in a silicate glass. 5–10 mol% increase in alkali oxide decreases T_g by 30–270 °C and T_s by 60–300 °C for Na_2O–Al_2O_3–SiO_2 and Na_2O–CaO–Al_2O_3–SiO_2 glasses [46,47]. 5 mol% increase of Na_2O decreases T_g and T_s by ~270 °C (from 786 to 515 °C) and ~300 °C (from 910 to 607 °C), respectively, for a silicate glass [46].

Al_2O_3 is the most commonly used intermediate oxide, generally at 5–10 mol% for a seal glass. Al_2O_3 is a network former if the coordination number of Al^{3+} is four and a network modifier if the coordination number of Al^{3+} is five or six [14,26,20]. T_g and T_s increase if Al_2O_3 is a network former because of the higher degree of network connectivity and lower fraction of non-bridging oxygen. T_g and T_s decrease if Al_2O_3 is a network modifier because of lower degree of network connectivity and higher fraction of non-bridging oxygen. One study reports that T_g increases by 20 °C (625–645 °C) when the Al_2O_3 content increases from 9.5 to 17 mol% in a SrO–Al_2O_3–La_2O_3–B_2O_3–SiO_2 glass [37]. Another study shows that T_g decreases by 30 °C (from 638 to 608 °C) in a CaO–MgO–borosilicate glass when the Al_2O_3 content increases from 6.9 to 17.0 mol% [45].

Several additives such as rare earth metal oxides and transition metal oxides are used in seal glass compositions to tailor the thermal properties. La_2O_3, a rare earth metal oxide, is commonly used in seal glass compositions. Less than 10 mol% La_2O_3 is sufficient to increase T_g by 30–50 °C although more than 20 mol% has been used in some seal glasses [27,32,42,48]. ZrO_2, TiO_2, NiO, ZnO, and Y_2O_3 are common transition metal oxides in seal glass compositions. The effect of transition metal oxides on T_g and T_s depends on the specific glass composition [17,22]. T_g and T_s increase when these oxides are network formers and decrease or stay unchanged when these oxides are network modifiers. For example, 2 mol% ZrO_2 addition has no effect on T_g in MgO–borosilicate glasses [36] but 3 mol% ZrO_2 addition increases T_g by 15–20 °C in a BaO–borosilicate glass [38] and T_s by 50–70 °C in an alkali and alkaline earth oxide-containing silicate glass [31]. Similar anomaly has been observed for TiO_2, Ni, and ZnO when they are added in silicate and borosilicate glasses [28,31,33,36,38,49–53].

The CTE of a seal glass should not differ by more than $1 \times 10^{-6}\,K^{-1}$ with the interfacing SOFC components in order to obtain pore- and crack-free interface [54]. CTE mismatch between the seal glass and the adjoining SOFC components can cause tensile ($CTE_{component} > CTE_{glass}$) or compressive ($CTE_{component} < CTE_{glass}$) thermal stress at the interface [55]. The CTEs of SOFC components are generally $10.5 \times 10^{-6}\,K^{-1}$ for the electrolyte, $12.4 \times 10^{-6}\,K^{-1}$ for the cathode, $10–14.0 \times 10^{-6}\,K^{-1}$ for the anode, and $11.0–15.0 \times 10^{-6}\,K^{-1}$ for the interconnect [56–58]. Cracks and pores may form at the interface due to tensile stress and a seal glass may delaminate from the interfacing components due to compressive [55] or shear stress. In practice, a CTE of $10.0–12.0 \times 10^{-6}\,K^{-1}$ is required for a seal glass.

Regarding glass network formers, CTEs of $9.0–13.0 \times 10^{-6}\,K^{-1}$, $9.5–10.5 \times 10^{-6}\,K^{-1}$, and $9.0–13.0 \times 10^{-6}\,K^{-1}$ have been obtained for silicate, borate, and borosilicate glasses, respectively [27–32,34,35,37–39,41–43,59–61]. For borosilicate glasses, CTE increases by $1.0–2.0 \times 10^{-6}\,K^{-1}$ with increase in B_2O_3/SiO_2 ratio as shown in Fig. 2 for a SrO–Al_2O_3–La_2O_3–B_2O_3–SiO_2 seal glass. The higher CTE of pure B_2O_3 glass ($14.4 \times 10^{-6}\,K^{-1}$), the asymmetric structure of borate structural groups, and the decrease in the network connectivity are the reasons for the CTE increase [14,16].

Regardless of modifier types, desired CTE has been obtained for seal glasses [27–32,34,35,37–39,41–43,59–61]. CTE increases with increasing modifier content and decreasing modifier field strength. For example, CTE increases from 8.5×10^{-6} to $12.0 \times 10^{-6}\,K^{-1}$ for a BaO–MgO–silicate glass when BaO/MgO ratio increases from 0.67 to 4.0 because of the lower field strength of BaO [29]. CTE increases from $\sim 8.0 \times 10^{-6}$ to $11.5 \times 10^{-6}\,K^{-1}$ for a BaO–borosilicate glass with BaO content increase from 20 to 40 mol% [43,62]. CTE increases from 8.08×10^{-6} to $9.20 \times 10^{-6}\,K^{-1}$ for a SrO–borosilicate glass when the SrO content increases from 35.31 to 41.76 mol% [32].

Intermediate oxides play a dual role in affecting CTE. For example, CTE decreases when Al_2O_3 is a network former and increases when it is a network modifier. 1–2 mol% Al_2O_3 addition decreases CTE by $\sim 1.5 \times 10^{-6}\,K^{-1}$ for silicate and borosilicate seal glasses [49,50]. 0.5–1.5 mol% Al_2O_3 addition decreases CTE by $\sim 0.2 \times 10^{-6}\,K^{-1}$ for a Na_2O–CaO–SiO_2 glass [63]. However, less than 0.5 mol% Al_2O_3 addition increases CTE by $\sim 0.2 \times 10^{-6}\,K^{-1}$ for the same Na_2O–CaO–SiO_2 glass system [63].

The effect of additives on CTE has no consistent trend. 2.0–3.0 mol% La_2O_3 increase in BaO–borosilicate and SrO–borosilicate seal glasses increases the CTE by $\sim 1.0 \times 10^{-6}\,K^{-1}$ due to increased amount of non-bridging oxygen [32,38]. Addition of transitional metal oxides increases CTE if they are network modifiers and decreases CTE if they are network formers. 3 mol% NiO increases CTE by $\sim 1.0 \times 10^{-6}\,K^{-1}$ for a BaO–borosilicate glass [38]. 2 mol% ZrO_2 decreases CTE by $0.5–0.7 \times 10^{-6}\,K^{-1}$ for a silicate glass [31] and a BaO–borosilicate glass [38] but has no impact for a MgO–borosilicate glass [36]. Similar anomalies have been observed for NiO addition in borosilicate glasses [36,38,51].

Required T_g, T_s, and CTE have been obtained in a wide range of silicate, borate, and borosilicate glasses as shown in Fig. 3 [28–31,35–42,47,49,50,59–61,64,65]. Silicate and borosilicate glasses (1–3 mol% B_2O_3) can be used as high temperature SOFC seals. Silicate, borate, and borosilicate glasses (≥5 mol% B_2O_3) can be used as intermediate and low temperature seals. A wide range of silicate, borate, and borosilicate glasses are suitable as SOFC seals regardless of operating temperatures from CTE point of view. Seal glasses for intermediate temperature SOFCs are the most thoroughly investigated. More research is needed for low temperature seal glasses in consideration of the recent development of low temperature SOFCs. Borate glasses are the most common low temperature SOFC seal glasses.

4.2. Devitrification resistance

Devitrification of a seal glass is undesirable because of the glass property change it incurs. Localized stresses due to the CTE difference between the devitrified phase(s) and the glass phase

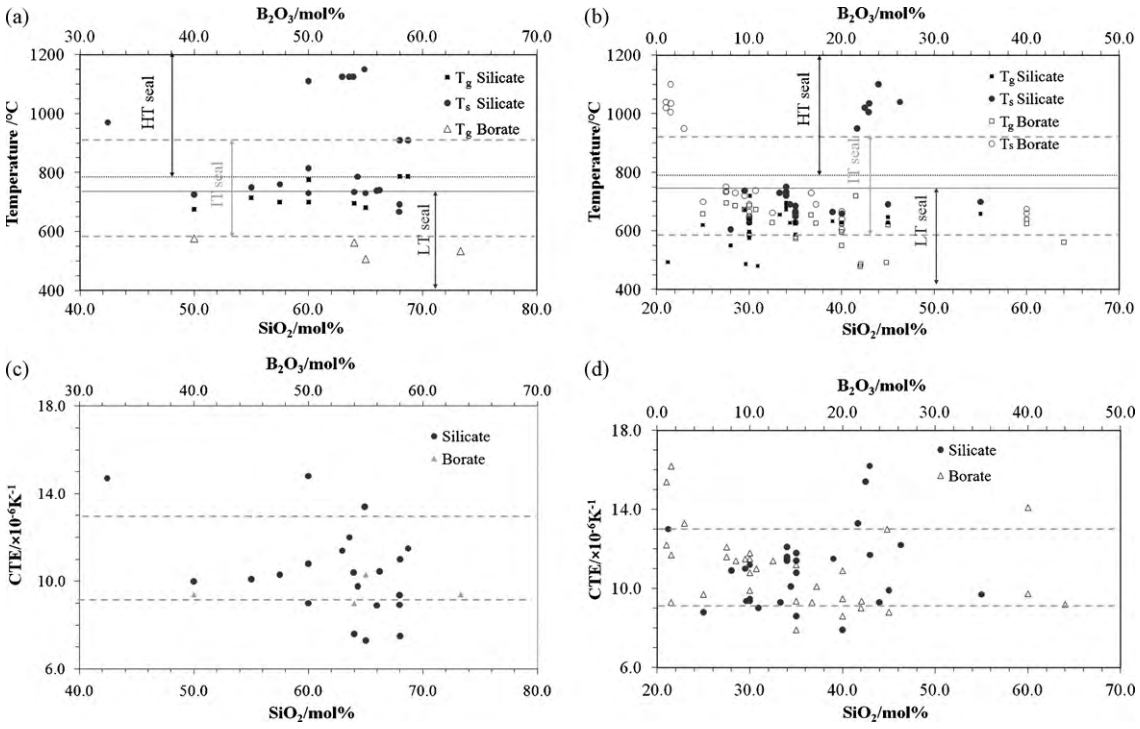

Fig. 3. Thermal properties of seal glasses as a function of network former contents [28–31,35–42,47,49,50,59–61,64,65]: (a) T_g and T_s of silicate and borate glasses, (b) T_g and T_s of borosilicate glasses, (c) CTE of silicate and borate glasses, and (d) CTE of borosilicate glasses. Desired CTE is marked by dotted lines. HT seal, IT seal, and LT seal indicate high temperature seal, intermediate temperature seal, and low temperature seal, respectively.

are of most concern. These stresses and the lower flowability of the devitrified phases can create pores and cracks in the glass and at the interface. For example, pores and cracks form in a BaO–CaO–borosilicate glass after thermal treatment at 850 °C for 1 h followed by 4 h at 750 °C because of the CTE difference between the devitrified phases and the glass phase [66]. Unfortunately, devitrification resistance is not well defined so far. Qualitatively, higher temperature and longer time required for a glass to devitrify mean higher devitrification resistance.

The origins of devitrification are the very small nuclei formed during glass making, heterogeneity in glass network structure, surface flaws, and residual stress from mechanical polishing [18,21,27,33,44,67,68]. Devitrification resistance depends on seal glass composition. Effect of network formers, modifiers, intermediates, and additives will be discussed to illustrate the effect of composition on the devitrification resistance. Thermal treatment conditions also affect the devitrification resistance. Devitrification due to nuclei formation during glass making and surface flaws is beyond the scope of the present discussion.

Glass network formers can degrade the devitrification resistance of a seal glass in two ways. First, the degree of network connectivity decreases with increased fraction of non-bridging oxygen-containing structural units. Second, coexistence of several different types of structural units induces heterogeneity in a glass network structure [16,44,69–74]. Silicate glasses have a higher degree of devitrification resistance than borate and borosilicate glasses because of their higher glass network connectivity, as demonstrated in Fig. 4 [28,38]. An increase in the B_2O_3/SiO_2 ratio also increases the content of BO_4 structural units, which do not mix homogeneously with silicate structural units. As a result, glass devitrification resistance decreases. In our work, the B_2O_3/SiO_2 ratio effect on the devitrification resistance of a $SrO–La_2O_3–Al_2O_3–B_2O_3–SiO_2$ system has been investigated [33,44]. At 850 °C, the devitrified phases appear at ≤50 h of thermal treatment time when B_2O_3 is present. For a B_2O_3-free glass composition, there is no devitrification after 200 h at 850 °C. Devitrification of a lithium disilicate glass occurs due to the presence of pyrosilicate (Si_2O_7) and orthosilicate (SiO_4) structural units, which cause glass structure heterogeneity [71,72,73].

Devitrification resistance of a seal glass also depends on glass modifiers. Fig. 5 shows the devitrification temperature of silicate and borosilicate glasses when alkaline earth oxides are used as glass network modifiers [29,36,60,75]. In these glasses, the overall composition is fixed but the type of modifier is varied. Devitrification temperature decreases in silicate glasses in the order of $Ba^{2+} > Sr^{2+} > Ca^{2+} > Mg^{2+}$ but increases in a borosilicate glass in the order of $Ba^{2+} < Ca^{2+} < Mg^{2+}$ (Fig. 5). Generally, heterogeneity in a glass structure increases with modifier field strength [76].

A small amount (<10 mol%) of intermediates in a seal glass generally improves devitrification resistance [77]. In a borosilicate glass, 3–8 mol% Al_2O_3 improves the devitrification resistance by decreasing the amount of borate structural units, which are immiscible with silicate structural units [78,79]. If an excess amount of intermediate exists, it decreases the devitrification

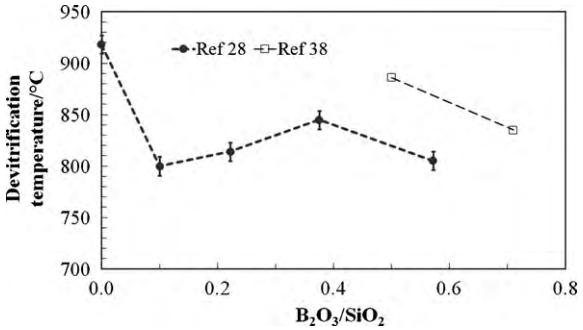

Fig. 4. Devitrification temperature change with B_2O_3/SiO_2 ratio in alkaline earth borosilicate glasses [28,38].

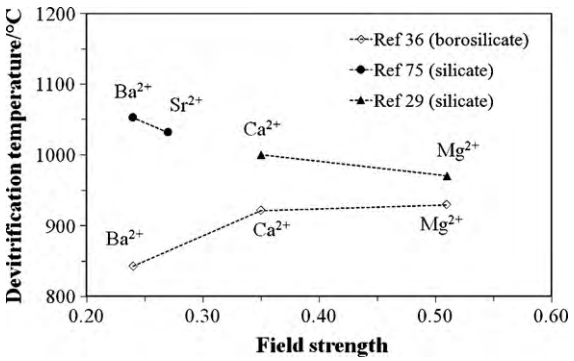

Fig. 5. Devitrification temperature vs. field strength of modifier cations in silicate and borosilicate glasses [29,36,75].

resistance. For example, 10 mol% Al_2O_3 degrades devitrification resistance by enhancing phase separation in a MgO–borosilicate glass [36].

Additives generally degrade devitrification resistance. In a BaO–borosilicate glass, 5 mol% La_2O_3 leads to the formation of $Ba_4La_6O(SiO_4)_4$ at 800 °C [38]. In SrO–borosilicate glasses, La_2O_3 (3–25 mol%) causes the formation of $LaBO_3$, Sr-containing lanthanum borate, and $La_2Si_2O_7$ phases at 800–1000 °C [27,32,33,37,44,68]. Effect of transition metal oxides on devitrification is specific to the glass composition. Devitrification resistance can be improved if transition metal oxides participate in the glass network and degraded if otherwise. Initial addition of TiO_2 decreases devitrification temperature of a MgO–borosilicate glass (2 mol% TiO_2) [36] and a borate glass (5 mol% TiO_2) [61] as shown in Fig. 6. Further addition of TiO_2 increases devitrification temperature in these glasses. In contrast, TiO_2 addition promotes devitrification in another MgO-containing glass due to glass composition difference [80]. Similar observations are made for ZrO_2 and ZnO additions in seal glasses [26,33,36,38]. ZrO_2 increases the devitrification resistance of BaO–borosilicate and MgO–borosilicate glass systems. ZnO, however, decreases the devitrification resistance of a BaO–MgO–borosilicate glass [28]. Transition metals play a similar role as transition metal oxides since they are oxidized in a seal glass. One most common example is Ni. For example, the devitrification temperature increases by 80 °C in a MgO–borosilicate glass with 2 mol% Ni addition [36]. However, the devitrifictaion time decreases by ~70 h with 2 mol% Ni addition in a $SrO–La_2O_3–Al_2O_3–B_2O_3–SiO_2$ glass [33].

Devitrification resistance of a seal glass also depends on heating rate, thermal treatment time, particle size, and exposed atmosphere of the glass. Devitrification temperature increases with heating rate. For example, the devitrification temperature of a BaO–silicate glass increases from 994 to 1062 °C when the heating rate increases from 2.5 to 40 °C min^{-1} [26]. The extent of devitrification increases with thermal treatment time until a stable state is reached. For example, the devitrification of a BaO–CaO–borosilicate glass increases from ~50% to ~70% after 120 h of thermal treatment in air at 750 °C and stays constant afterwards [41]. Smaller particle sizes decrease the devitrification temperature. For example, the devitrification temperature decreases from 910 to 833 °C when the particle size decreases from 500–850 to <20 μm for a MgO–BaO–silicate glass [25]. The effect of atmosphere will be discussed in Section 5.1.

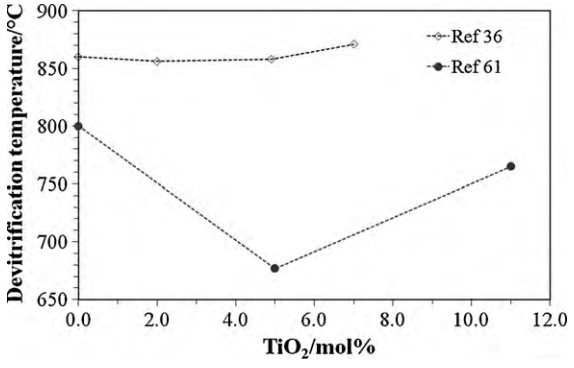

Fig. 6. Devitrification temperature change with TiO_2 content in borate and borosilicate seal glasses [36,61].

4.3. Electrical resistivity

The electrical resistivity of a seal glass depends on the composition and should be $>10^4$ Ω cm in order to avoid shunting [81]. The effects of network former and modifier oxides are known but the effects of intermediates and additives are uncertain because of their different roles in a specific glass composition. The electrical resistivity of borate glasses is higher than that of silicate glasses due to 'boron anomaly' [14]. The electrical resistivity of a Na_2O–silicate glass increases with initial addition but decreases with further addition of intermediate oxides, probably due to the 'combined ion effect' [18]. Alkaline earth oxide-containing glasses generally have $>10^4$ Ω cm electrical resistivity, which increases with ionic radius and valence of the modifier ions [15,18]. For example, the electrical resistivity of a BaO–ZnO–silicate glass (~1.3×10^9 Ω cm) is ten times higher than that of a BaO–MgO–silicate glass (~5.8×10^8 Ω cm) due to the larger ionic radius of Zn^{2+} ions [81].

Devitrification affects electrical resistivity but the exact trend depends on the composition and morphology of the devitrified phases in a glass matrix. For example, Na_2O- and B_2O_3-rich and conductive regions (~50 nm) are isolated in an insulating SiO_2 matrix in a $Na_2O–B_2O_3–SiO_2$ glass. As a result, the electrical resistivity of the phase-separated $Na_2O–B_2O_3–SiO_2$ glass is higher (~10^{13} Ω cm) than that of the original seal glass (~10^6 Ω cm) [82]. In contrast, the electrical resistivity of a $BaO–ZnO–SiO_2$ glass decreases from 1.3×10^9 to 1.0×10^6 Ω cm and that of a $BaO–MgO–SiO_2$ glass from 5.8×10^8 to 10^6 Ω cm due to devitrification [81].

5. Seal glass interaction in solid oxide fuel cells

5.1. Interaction with different atmospheres

Different types of fuels can be used in SOFCs, such as hydrogen, syngas, and hydrocarbons [83]. Seal glasses are simultaneously exposed to oxidizing and reducing atmospheres at high temperatures during SOFC operation. The reducing atmosphere at the anode can also contain a high water content. In this context, atmospheres can adversely affect the properties of a seal glass by vaporizing glass constituents, changing glass microstructure, and accelerating glass devitrification. The effect of air on seal glasses is better understood because many studies are conducted in air atmosphere. In contrast, the effect of reducing atmospheres on seal glasses has not been well studied.

Vaporization of glass constituents changes glass composition and can adversely affect the desired thermal, chemical, and electrical properties. Pure silica glass does not vaporize in dry air due to its high melting temperature but vaporizes in the form of $Si(OH)_4$ species by reacting with H_2O and in the form of SiO species by reacting with H_2 at 1000 °C. Also, $Si(OH)_4$ species dominates in H_2O-containing reducing atmosphere at high temperatures [84]. B_2O_3 has a higher tendency to vaporize at SOFC operating temperatures due to its low melting temperature and high vapor pressure. Vaporization of B_2O_3 from a seal glass is more dominant in the

presence of water. Boron reacts with water and vaporizes in the form of HBO_2 gaseous species in alkali oxide-free glasses and in the form of RBO_2 (R = Na, K) and $B(OH)_3$ species in alkali oxide-containing glasses [85,86]. For an alkaline earth oxide-containing borosilicate seal glasses thermally treated at 800 °C for 168 h, the weight loss due to gaseous $B_3H_3O_6$ vaporization increases from 0.16 to 0.98 mg cm^{-2} when the atmosphere is changed from oxidizing atmosphere to 30% H_2O/H_2 atmosphere. For this glass, the weight loss increases from 0.03 to 0.16 mg cm^{-2} as the B_2O_3 content increases from 2 to 20 mol% [87]. Alkali oxide-containing borate glass and borosilicate glass vaporize in the form of gaseous borates and alkali/alkaline earth metaborates [88]. As a rule of thumb, alkali oxides and boron oxide should not be used as seal glass constituents in order to minimize vaporization. Generally, alkaline earth oxide modifiers and intermediate oxides do not vaporize [14]. For example, weight loss is negligible for a $SrO–La_2O_3–Al_2O_3–SiO_2$ seal glass after thermal treatment in 50% H_2O/H_2 at 800 °C for 1000 h [68].

Phase separation in a seal glass leads to undesirable devitrification. A glass can phase separate by reacting with water. BaO- and Na_2O-containing silicate glasses tend to interact with water and form silica-rich secondary phases [89,90]. Al_2O_3 and transition metal oxides can hinder phase separation [14,91]. SOFC atmospheres also affect phase separation. Devitrification of a $SrO–La_2O_3–Al_2O_3–SiO_2$ seal glass is observed when thermally treated at 800 °C for 1000 h in air but not in 50% H_2O/H_2 atmosphere [68]. Changes of devitrification resistance with atmosphere can be understood from different types of devitrified phases. Sr_2SiO_4, Al_2SiO_5, and $Sr_7Al_{12}O_{25}$ phases evolve when a $SrO–La_2O_3–Al_2O_3–SiO_2$ seal glass is thermally treated in air but Sr_2SiO_4, $La_{9.33}Si_6O_{26}$, and $Sr_{12}Al_{14}O_{33}$ phases evolve when the glass is thermally treated in 50% H_2O/H_2 [68]. The nucleation temperature of a $Li_2O–Al_2O_3–SiO_2$ glass decreases from 610 to 570 °C when 3.07 at% N_2 is present in the glass [92].

5.2. Interaction with different solid oxide fuel cell components

A seal glass should wet and bond with electrolyte, electrodes, and metallic interconnects uniformly to form good sealing without any pores or cracks at the interface. The interaction usually involves inter-diffusion and chemical reaction of the elements of the seal glass and the interfacing cell components [93,94]. Severe interaction between the seal glass and the adjacent cell components increases interfacial layer thickness, which in turn leads to pore and crack formation at the interface and delamination of the glass [55,94]. There is no consensus on desired interfacial layer thickness. A layer less than 10-μm thick may be acceptable.

Interaction of a seal glass with metallic interconnect is more severe than with other cell components [93]. Subsequently, seal glass interaction with metallic interconnect has been the focus of most interfacial studies. Chromia forming ferritic stainless steel is the most preferred interconnect [5], which contains 17.0–33.0 wt% Cr with different trade names such as Crofer 22 APU, AISI 446, AISI 430, and AL29-4C alloys [95]. Seal glass interaction with interconnect depends on the glass and interconnect compositions, exposed atmospheres, and sealing conditions. For example, a BaO–CaO–borosilicate glass forms a porous interface with cracks with the Crofer 22 APU alloy but pore- and crack-free interface with a slightly different alloy composition [34,96].

B_2O_3 in a seal glass favors bonding with interconnect alloys because of its good wetting behavior but the extent of diffusion and chemical reaction may be high [28,47,97]. For example, more than 15 mol% B_2O_3 is required for BaO–MgO–silicate and BaO–ZnO–silicate glasses to bond with the Crofer 22 APU alloy [28]. But the interfacial layer thickness increases from 1–2 to ~20 μm when 10 wt% B_2O_3 is added to a $Na_2O–CaO–$silicate glass to bond with the AISI 430 alloy [47,97].

Presence of alkali oxide(s) in a seal glass is undesirable. An alkali silicate glass can react with an interconnect and form alkali chromates (such as Na_2CrO_4, K_2CrO_4), which vaporize and destabilize glass network [98,99]. The bonding of alkaline earth oxide-containing glasses with interconnect, however, is dependent on the glass network formers. On the one hand, $SrO–La_2O_3–Al_2O_3–SiO_2$ and BaO–CaO–silicate glasses bond well with the Crofer 22 APU alloy and form 1–3 μm thick interfaces that are stable for 500–1000 h at 800 °C [100–102]. On the other hand, alkaline earth borosilicate glasses bond with the Crofer 22 APU alloy at 850 °C but form 1–3 μm thick interface with extensive cracks followed by a 2–3 μm thick porous layer [35,96]. The origin of the porous layer and cracks at the interface is two-fold. First, devitrification causes glass volume decrease, poor glass flow at the interface, and CTE mismatch between the glass phase and the devitrified phases. Second, the glasses react with the volatile chromium species such as CrO_3 and $CrO_2(OH)_2$ from the interconnect and form $BaCrO_4$ and $SrCrO_4$ [35,96]. The CTEs of these chromate phases ($21.0–23.0 \times 10^{-6}\ K^{-1}$) are much higher than those of the seal glasses ($10.0–12.0 \times 10^{-6}\ K^{-1}$). These interfaces of borosilicate glasses are also unstable. For example, the interfacial layer thickness of a BaO–CaO–borosilicate glass with the Crofer 22 APU alloy increases from 10 to 76 μm after 200 h of thermal treatment at 750 °C in air due to severe interaction [103].

Effect of additives on the seal glass bonding with metallic interconnect is not well understood. A BaO–CaO–borosilicate glass does not bond with the Crofer 22 APU alloy if minor amounts of La_2O_3 and ZnO are present in the glass [34]. However, other seal glasses bond with the Crofer 22 APU alloy well even if La_2O_3 is present [100,101]. Transition metal oxides such as NiO and ZnO disrupt the network structure in alkaline earth borosilicate glasses and form interfaces with pores and cracks [28,51].

Interaction of seal glass with metallic interconnect and the interfacial stability are also affected by atmosphere. For example, a BaO–MgO–silicate glass does not bond with the Crofer 22 APU alloy in an oxidizing atmosphere but bonds well with the same alloy in a H_2O/H_2 atmosphere [104]. Chromium from the Crofer 22 APU alloy diffuses ~10 μm into a $SrO–La_2O_3–Al_2O_3–SiO_2$ glass in air but diffuses ~6 μm in 50% H_2O/H_2 atmosphere. In simultaneous oxidizing and reducing atmospheres, nodular iron rich oxides form on the air side and chromia forms on the hydrogen side for an interconnect material similar to the Crofer 22 APU alloy [105,106]. These oxide layers are conductive and grow extensively (300–500 μm) at 800 °C with time (400–500 h) to cause electrical shunting [105,106].

Seal glasses generally wet ZrO_2 electrolyte well. Interfacial stability between a seal glass and ZrO_2 electrolyte is not a problem regardless of glass composition, sealing condition, and atmosphere [30,32,34,38,43,104]. There are a few cases that a seal glass interacts with the electrolyte. For example, a BaO–CaO–borosilicate glass reacts with yttria stabilized zirconia and forms $BaZrO_3$ after 1200 h of thermal treatment at 750 °C [39]. 15 vol% NiO-containing SrO–CaO–borosilicate seal glass shows an accumulation of NiO particles and reduction of NiO to metallic Ni near the interface in 30% H_2O/H_2 atmosphere after 24 h of thermal treatment at 800 °C [51]. Nonetheless, seal glass/ZrO_2 electrolyte interfacial stability is not a major concern.

Interaction between electrodes and seal glass can change the morphology of the electrodes [107–111]. One study shows that a silica layer of 0.4–0.6 μm from a Na_2O-silicate seal glass segregates at the anode and electrolyte interface and covers the nickel particles in the anode. Distribution of nickel particles and pores in the anode may have changed due to the interaction with this seal glass [107]. Another report shows that a $Na_2O–$borosilicate glass reacts with the cathode and causes the cathode grains to coarsen from 0.69 to 1.13 μm [109]. Larger grain size and uneven distribution of grains and pores in the cathode degrade cell performances

due to decreased number and length of triple phase boundaries. An electrically insulating layer can also form at the interface of electrode–electrolyte when a seal glass reacts with electrodes. Since the above studies have been conducted for alkali oxide-containing seal glasses, silica segregation at the anode–electrolyte interface and the coarsening of the cathode grains may be due to the interaction between the vaporized species of the seal glasses and the electrodes. More research should be conducted to understand this problem.

5.3. Sealing condition

Interfacial stability can be improved by controlling sealing conditions such as heating rate, sealing temperature and atmosphere, preoxidation of the interconnect, and coating of an oxide layer on the interconnect. A slow heating rate during sealing is beneficial. For example, porosity and pore size at the interface decrease when the heating rate decreases from 25 to 5 °C min^{-1} for a Na_2O–CaO–silicate glass [30]. Increasing sealing temperature (>900 °C) improves the interfacial stability for a SrO–CaO–borosilicate glass by hindering $SrCrO_4$ phase formation at the interface [51]. Sealing of a SrO–La_2O_3–Al_2O_3–SiO_2 glass with the Crofer 22 APU alloy in argon atmosphere hinders $SrCrO_4$ formation at the interface [100,101]. Preoxidation of interconnect at 800–1000 °C introduces an oxide layer and enhances the bonding with seal glass. The possible reasons are twofold. First, the oxide layer acts as a transition layer with a CTE between those of the interconnect and the seal glass. The residual stress due to CTE mismatch is decreased. For example, a 1–5 μm thick chromium–manganese–iron oxide layer on the preoxidized AISI 430 alloy facilitates bonding with a Na_2O–CaO–silicate seal glass [97]. Second, the oxide layer decreases the contact angle between the seal glass and the interconnect and leads to better adhesion. For example, preoxidation of the AISI 430 alloy and the Crofer 22 APU alloy at 800–1000 °C for 2 h decreases pores and cracks at the interface [112]. However, a thick oxide layer can cause spallation of seal glass [112]. Coating the interconnect with an oxide layer improves the interfacial stability by increasing adhesion and eliminating the direct contact of the interconnect with harsh environments. For example, NiO, Co_3O_4, Al_2O_3, and ZrO_2 coatings on the Crofer 22 APU alloy improve the bonding and interface stability by improving adhesion and eliminating chromate and iron oxide formation at the interface [99,113].

5.4. Thermomechanical properties

A seal glass should withstand 14–35 kPa pressure due to gas flow, vibration, and thermal cycling during SOFC operation [10,103]. It should also withstand more than 100 thermal cycles for stationary applications and more than 1000 thermal cycles for mobile applications [13]. Generally, higher strength is obtained in a glass with higher T_g. Elastic modulus of 30–100 GPa can be obtained in a seal glass [114]. Devitrification can either decrease or increase the elastic modulus of a seal glass depending on the specific composition. For a BaO–CaO–borosilicate seal glass, elastic modulus decreases from 78.0 to 60.8 GPa after 1000 h of thermal treatment at 750 °C due to devitrification [115]. In contrast, the shear strength of a BaO–CaO–silicate seal glass with the Crofer 22 APU alloy increases from 0.3 to 4 MPa due to glass devitrification [116,117].

Thermomechanical stress, σ, can be defined as

$$\sigma = \Delta E \cdot \Delta\alpha \cdot \Delta T \quad (2)$$

where ΔE, $\Delta\alpha$, and ΔT are the difference in elastic modulus, CTE, and temperature, respectively, between the glass and the interfacing components [94]. Initiation and growth of cracks at the interface occur if the thermomechanical stress exceeds the tensile strength of seal glass or the interfacial bonding strength. Excessive compressive [55] or shear stress delaminates the seal glass from the interface. Thermal cycling induces thermomechanical stress due to temperature gradient and change in material properties with temperature. Thermal stress effect is more severe than mechanical stress effect for crack initiation and growth [118]. Accordingly, thermomechanical properties of the interface should be discussed from interfacial bonding strength point of view. The bonding strength depends on glass composition and sealing condition. High interfacial bonding strength is desired in order to avoid failure at the interface but the desired value is unknown. Seal glass/interconnect interfacial strength of 2.0–8.5 MPa has been achieved [112,113,119]. Alkali oxide-containing seal glasses have lower interfacial strength than alkaline earth oxide-containing seal glasses [112,116,119]. The interfacial bonding strength of Na_2O-silicate and SrO–CaO–borosilicate glasses with the Crofer 22 APU interconnect alloy is ~2.0 and 7 MPa, respectively. Higher field strength and charge of alkaline earth oxides hinder the rotational movement of glass structural units and result in higher elastic modulus. As a result, the mismatch in the elastic moduli between the seal glass and the interconnect deceases and the interfacial strength increases.

Sealing atmosphere and protective coating on the interconnect change the interfacial strength by changing the interfacial morphology. For example, thermal aging of a SrO–CaO–borosilicate glass/Crofer 22 APU alloy couple in air for 500 h at 850 °C decreases the interfacial strength from 6.9 to 0.5 MPa due to the formation of $SrCrO_4$ phase. $SrCrO_4$ induces thermal stress and results in pores and cracks at the interface [112]. An Al_2O_3 coating of 50–100 μm thick on the Crofer 22 APU alloy hinders strontium chromate formation and increases the bonding strength from 6.9 to ~8.5 MPa after aging in air at 850 °C for 300 h [113].

Seal glass configuration also affects the interfacial strength [120]. A smooth and thin seal glass layer can improve the interfacial strength by reducing the thermomechanical stress. For example, a seal glass layer thicker than 250 μm almost always leads to sealing failure according to numerical calculation [120].

Limited literature reports are available for the thermal cycling resistance of a seal glass/interconnect assembly. A silicate seal glass sandwiched between the Crofer 22 APU alloy and the zirconia electrolyte has withstood 300 thermal cycles at 3 °C min^{-1} heating rate [24]. A SrO–La_2O_3–Al_2O_3–SiO_2 glass sandwiched between the AISI 441 alloy and the zirconia electrolyte has withstood 100 thermal cycles at 20 °C min^{-1} heating rate. A BaO–CaO–borosilicate seal glass/Crofer 22 APU sample, however, withstands only 40 thermal cycles at 75 °C min^{-1} [102]. Localized stress due to devitrification of the glass and severe interaction with the Crofer 22 APU alloy during thermal cycling contribute to poor thermal cycling resistance.

6. Sealing performance

Sealing performance is the ability to prevent mixing and leakage of gasses. Gas leakage can be internal or external and should be less than 1% of the fuels used during the entire cell operation [9]. However, currently there is no agreed procedure for sealing performance evaluation. Four different gas leakage units are reported in literature: sccm/cm (standard cubic centimeters per minute per centimeter), Pa L s^{-1}, Pa m^2 s^{-1}, and L min^{-1} [34,99,121,122]. Sealing performance of different seal glasses is not comparable because of limited literature reports, non-standardized testing methods, and widely varied leakage rate expressions. Nonetheless, sealing performance is most commonly evaluated by a pressure-leakage test [9]. In this method, a seal glass is sandwiched between two cell components such as interconnect and electrolyte to form a tri-layer

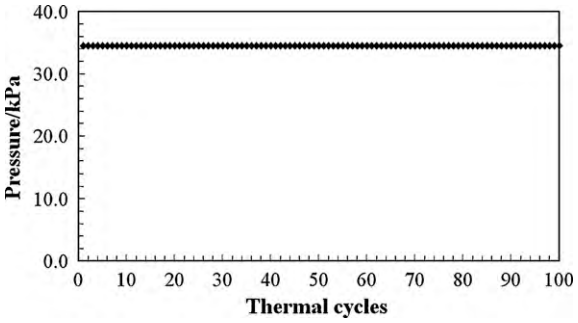

Fig. 7. Sealing performance of a $SrO–La_2O_3–Al_2O_3–SiO_2$ glass.

assembly, which is subjected to a differential pressure of 14–35 kPa to simulate the gas flow in a typical SOFC [102].

Pores and cracks at the interface and in the seal glass are gas leakage paths. Localized thermomechanical stress due to the devitrification of the seal glass and severe interaction with the interfacing components increase the numbers of pores and cracks and gas leakage rate. For example, the leakage rate increases from 10^{-3} to 10^{-4} sccm cm^{-1} to $1–2 \times 10^{-2}$ sccm cm^{-1} for a SrO–CaO–borosilicate seal glass due to the presence of pores and cracks [51]. Even though sealing performance has been evaluated with a slow heating and cooling rate of 3–5 °C min^{-1} for some studies [24,34,51,99], it should be emphasized that a seal glass should withstand thermal cycles with quick start-up and shut-down. Quick start-up is required, for mobile applications in particular, to reach the operating temperature quickly. Quick shut-down is required to avoid explosions due to malfunctioning of SOFC units. For example, the leakage rate of a BaO–borosilicate glass increases by an order of magnitude during cooling from 700 °C (10^{-3} sccm cm^{-1}) to 100 °C (3×10^{-2} sccm cm^{-1}) because of extensive crack growth [123]. We have evaluated the sealing performance of the $SrO–La_2O_3–Al_2O_3–SiO_2$ glass as a function of thermal cycles from room temperature to 800 °C with a heating rate of 20 °C min^{-1}. The sealing performance is shown in Fig. 6 as a function of thermal cycles with 34.5 kPa differential pressure. The $SrO–La_2O_3–Al_2O_3–SiO_2$ glass has withstood 100 thermal cycles before the leakage test was aborted (Fig. 7). The seal glass might be able to perform for many more thermal cycles if continued.

7. Impact of seal glass on performance and durability of solid oxide fuel cells

Seal glass failure degrades the performance and durability of SOFCs by affecting the microstructure stability of the electrodes. Deposition of vaporized glass species on electrode grains or at grain boundaries and changes in overall compositions of electrodes and seal glass are common issues. 2% performance degradation is observed in an anode supported cell after 1300 h at 850 °C [107]. Insulating Si-containing phases of 10–600 nm thickness from a Na_2O-silicate seal glass segregate at the anode–electrolyte interface and around the Ni particles [124]. These insulating phases increase ohmic and polarization resistances, change the Ni particle size and distribution, and decrease the electrochemically active sites. A SiO_2 insulating layer also decreases the conductivity of Gd-doped CeO_2 electrolyte for low temperature SOFCs [125]. Increased H_2O content in the cell accelerates the degradation due to the blocking effect of oxygen migration and increase in area specific resistance [126]. H_2O effect on the degradation may partly be caused by accelerated $Si(OH)_4$ evaporation from the seal glass [107]. A Na_2O–borosilicate glass reacts with the cathode and increases the area specific resistance by ~0.02 Ω cm^2 after 144 h of thermal treatment at 1000 °C [109]. Alkali oxide-containing seal glasses enhance the evaporation of chromium from the interconnect and the deposition on the electrochemically active sides of the cathode.

Degradation of SOFC performance and durability can be accelerated if insulating phases at the electrode–electrolyte interfaces form from the interaction of the seal glass with the electrodes and electrolyte. A seal glass can alter the compositions of the electrodes by inter-diffusion [127]. In particular, oxygen diffusion from the seal glass can oxidize the Ni particles in the anode and diffusion of manganese and strontium from the cathode to the glass can degrade the cathode electrical conductivity. $La_2Zr_2O_7$ and $SrZrO_3$ insulating phases have been observed at the cathode–electrolyte interface [127]. Seal glasses generally contain La_2O_3, BaO, SrO, and CaO as the constituents. Subsequently, $La_2Zr_2O_7$ and $SrZrO_3$ may form due to the interaction of the seal glass with the anode and the electrolyte. Alkaline earth borate and borosilicate glasses react with the electrolyte at 800–900 °C and form $BaZrO_3$, $SrZrO_3$, $CaZrO_3$, and $CaZr_4O_9$ [39,59].

8. Future perspective

Desired thermal properties of SOFC seal glasses have been achieved in several glass systems but long-term stability remains a persistent problem. Lack of detailed understanding of composition–structure–property relations is the main issue in designing seal glass compositions. Quantitative analysis of network structure, such as the amounts of different structural units and non-bridging oxygen, and the coordination number of constituent cations, should be pursued. More detailed structural information such as cation-oxygen bond length and bond angles should be obtained.

The interfacial reactions depend on the seal glass composition and sealing conditions such as temperature and atmosphere. Interfacial reaction kinetics needs to be understood for different glass systems. Lack of thermodynamic data for different new phases formed at the interface hinders the understanding of the reaction kinetics. Detailed analysis of the interfacial compositions combined with thermodynamic modeling is required in order to address these issues. High resolution and in situ characterization techniques will greatly facilitate such studies.

The origins of localized stress have been expressed and modeled in terms of mismatch in CTE and elastic moduli. Morphology such as pore size and distribution and devitrified phases can potentially affect localized stress but have not been included in modeling. The thermal conductivity of seal glasses should be considered since thermal gradient contributes to localized thermal stress.

The performance and durability of SOFCs strongly depend on the seal glass thermomechanical properties such as interfacial strength. However, currently there is no standard procedure to measure the interfacial strength; the parameters and units for sealing performance evaluation are not clearly defined. As a result, the sealing performance of several seal glass systems cannot be compared. Differential pressure, seal thickness, leakage area, and gas volume in the tri-layer assembly significantly affect the sealing performance. The pressure-leakage test has been demonstrated to be a quicker method to evaluate sealing performance, generally in an inert atmosphere. Oxidizing and reducing atmospheres should be used for sealing performance evaluation because these atmospheres significantly affect the interfacial morphology.

In practice, fine seal glass powders (30–50 μm) are mixed with binders to obtain less than 1000 μm thick glass layer. Pores can form in the seal glass layer due to binder removal during sealing. Sealing performance can be improved by eliminating pore formation. Lower devitrification resistance of fine glass powders due to

high surface areas degrades the thermal and interfacial stability. Use of bulk glass of suitable dimensions can improve the thermal and interfacial stability. Raw material and fabrication cost database is needed from production point of view.

Current research trend is to reduce the operating temperature of SOFCs to <700 °C. Suitable seal glasses for low temperature SOFCs need to be developed. Borate glasses may be suitable as low temperature seal glasses but extensive research is yet to be done.

Seal glass should be stable for 5000–40,000 h for practical applications. The evaluation of seal glass stability for such a long period is not feasible for rapid seal development. A model needs to be developed to predict the life cycle of a seal glass.

9. Summary

Seal glass requirements and compositional design challenges are discussed for three types of glasses: silicate, borosilicate, and borate. Desired thermal properties have been obtained in all three types but devitrification resistance is better for silicate seal glasses. Borate and borosilicate glasses are not suitable seal glass in terms of long term stability. Alkali oxides are not desired in seal glass composition because of vaporization, low T_g, and low T_s. Borosilicate, borate, and alkali oxide-containing seal glasses tend to vaporize in the cell operating conditions but alkaline earth silicate seal glasses do not. Electrical resistivity of a bulk seal glass is generally $\geq 10^4\ \Omega$ cm and not a major concern. The interfacial stability with interconnect alloys depends on many factors such as composition and sealing conditions. Borosilicate glasses may facilitate bonding with interconnect alloys but degrade interfacial stability. Bonding strength and thermal cycling resistance degrade mainly due to thermal stress and strongly depend on the thermal properties and devitrification resistance of seal glass, and interfacial morphology and stability. Alkaline earth oxide-containing seal glass and surface modification of interconnect alloys improve bonding strength. Composition dependence on the thermal cycling resistance and sealing performance is not well understood because of the very limited studies. A $SrO–La_2O_3–Al_2O_3–SiO_2$ system has superior performance than other seal glasses reported in literature in terms of the desired thermochemical properties, sealing performance, and thermal cycling resistance.

Understanding the composition–structure–property relations of seal glass is the key for suitable seal glass compositional design. Lack of comprehensive compositional and structural studies is the major barrier. The reaction kinetics of a seal glass with interfacing components needs to be established since the interfaces play a critical role in the sealing performance. Mismatches in CTEs and elastic moduli between the seal glass and the interfacing components are the origin of thermomechanical stress. However, limited data are available in this regard.

To compare the performance of different seal glasses, a standard procedure needs to be established. Suitable seal glass systems for low temperature solid oxide fuel cells should be extensively studied.

Acknowledgment

Financial support of the Department of Energy under Award Number DE-FC07-06ID14739 is sincerely acknowledged.

References

[1] M. Yokoo, Y. Tabata, Y. Yoshida, K. Hayashi, Y. Nozaki, K. Nozawa, H. Arai, J. Power Sources 178 (2008) 59–63.
[2] M.C. Williams, Fuel Cells 7 (2007) 78–85.
[3] J.M. Ralph, A.C. Schoeler, M. Krumpelt, J. Mater. Sci. 36 (2001) 1161–1172.
[4] J.W. Fergus, Solid State Ionics 171 (2004) 1–15.
[5] W.Z. Zhu, S.C. Deevi, Mater. Sci. Eng. A 348 (2003) 227–243.
[6] EG & G Technical Services, Fuel Cell Handbook, seventh ed., US Department of Energy, Office of Fossil Energy, National Energy Technological Laboratory, Morgantown, West Virginia, 2004, chapter 7, pp. 7-1r-r7-49.
[7] F.P. Nagel, T.J. Schildhauer, S.M.A. Biollaz, A. Wokaun, J. Power Sources 184 (2008) 143–164.
[8] J.F.B. Rasmussen, P.V. Hendriksen, A. Hagen, Fuel Cells 8 (2008) 385–393.
[9] P.A. Lessing, J. Hartvigsen, S. Elangovan, in: J.W. Fergus, R. Hui, X. Li, D.P. Wilkinson, J. Zhang (Eds.), Solid Oxide Fuel Cells: Materials Properties and Performance, CRC Press, Taylor & Francis Group, Florida, 2009, pp. 213–237.
[10] K.S. Weil, J. Miner. Met. Mater. Soc. 58 (2006) 37–44.
[11] J.W. Fergus, J. Power Sources 147 (2005) 46–57.
[12] P.A. Lessing, J. Mater. Sci. 42 (2007) 3465–3476.
[13] D. Stolten, L.G.J.B.d. Haart, L. Blum, Ceram. Eng. Sci. Proc. 24 (2003) 263–272.
[14] H. Scholze, Glass Nature, Structure, and Properties, Springer–Verlag, New York, 1991, chapter 2, pp. 107–110, 136–143; chapter 3, pp. 164, 181–193, 297–303, 322–348.
[15] W.D. Kingery, H.K. Bowen, D.R. Uhlmann, Introduction to Ceramics, second ed., John Wiley and Sons, New York, 1976, chapter 3 pp. 91–122; chapter17, pp. 873–888.
[16] M.B. Volf, Chemical Approach to Glass, Glass Science and Technology, vol.7, Elsevier, Amsterdam, 1984, chapter 1, pp. 22–35, 43–58, 88–113; chapter 2, pp. 141–205, 280–302.
[17] G. Calas, L. Cormier, L. Galoisy, P. Jollivet, C R Chim. 5 (2002) 831–843.
[18] J.E. Shelby, Introduction to Glass Science and Technology, second ed., The Royal Society of Chemistry, Cambridge, 2005, chapter 5, pp. 76–100; chapter 8, pp. 166–176.
[19] J.E. Shelby, J. Appl. Phys. 47 (1976) 4489–4496.
[20] G.N. Greaves, S. Sen, Adv. Phys. 56 (2007) 1–166.
[21] W. Vogel, Structure and Crystallization of Glass, Pergamon, New York, 1971, p. 144.
[22] L. Galoisy, L. Cormier, S. Rossano, A. Ramos, G. Calas, P. Gaskell, M.L. Grand, Miner. Mag. 64 (2000) 409–424.
[23] P. Hrma, W.T. Han, A.R. Cooper, J. Non-Cryst. Solids 102 (1988) 88–94.
[24] R.N. Singh, Int. J. Appl. Ceram. Tech. 4 (2007) 134–144.
[25] M.J. Pascual, C. Lara, A. Durán, Eur. J. Glass Sci. Tech. B 47 (2006) 572–581.
[26] N.P. Bansal, M.J. Hyatt, J. Mater. Res. 4 (1989) 1257–1265.
[27] M.K. Mahapatra, K. Lu, R.J. Bodnar, Appl. Phys. A 95 (2009) 493–500.
[28] M.J. Pascual, A. Guillet, A. Durán, J. Power Sources 169 (2007) 40–46.
[29] C. Lara, M.J. Pascual, A. Duraĭn, J. Non-Cryst. Solids 348 (2004) 149–155.
[30] F. Smeacetto, M. Salvo, M. Ferraris, J. Cho, A.R. Boccaccini, J. Eur. Ceram. Soc. 28 (2008) 61–68.
[31] T.J. Kohli, R. Morena, Sealing frits, Euro. Patent 0982274A2 (2000).
[32] K.L. Ley, M. Krumpelt, R. Kumar, J.H. Meiser, I. Bloom, J. Mater. Res. 11 (1996) 1489–1493.
[33] M.K. Mahapatra, K. Lu, J. Power Sources 185 (2008) 993–1000.
[34] S. Ghosh, A.D. Sharma, P. Kundu, R.N. Basu, J. Electrochem. Soc. 155 (2008) B473–B478.
[35] Y.S. Chou, J.W. Stevenson, P. Singh, J. Electrochem. Soc. 154 (2007) B644–B651.
[36] N. Lahl, K. Singh, L. Singheiser, K. Hilper, D. Bahadur, J. Mater. Sci. 35 (2000) 3089–3096.
[37] M.K. Mahapatra, K. Lu, W.T. Reynonds Jr., J. Power Sources 179 (2008) 106–112.
[38] S.B. Sohn, S.Y. Choi, G.H. Kim, H.S. Song, G.D. Kim, J. Am. Ceram. Soc. 87 (2004) 254–260.
[39] K.D. Meinhardt, D.S. Kim, Y.S. Chou, K.S. Weil, J. Power Sources 182 (2008) 188–196.
[40] T. Yoshii, Sealing glass composition, sealing glass frit and sealing glass sheet, US Patent, 2006/0019813 A1 (2006).
[41] K.D. Meinhardt, J.D. Vienna, T.R. Armstrong, L.R. Pederson, Glass–ceramic joint and method of joining, US Patent 6532769 B1 (2003).
[42] I.D. Bloom, K.L. Ley, Compliant sealants for solid oxide fuel cells and other ceramics, US Patent, 5453331 (1995).
[43] S.B. Sohn, S.Y. Choi, G.H. Kim, H.S. Song, G.D. Kim, J. Non-Cryst. Solids 297 (2002) 103–112.
[44] K. Lu, M.K. Mahapatra, J. Appl. Phys. 104 (2008), 074910.
[45] R.E. Loehman, H.P. Dumm, H. Hofer, Ceram. Eng. Sci. Proc. 23 (2002) 699–705.
[46] J.G. Larsen, P.H. Larsen, C. Bagger, High temperature sealing material, Euro. Patent 1010675A1 (2000).
[47] F. Smeacetto, M. Salvo, M. Ferraris, V. Casalegno, P. Asinari, J. Eur. Ceram. Soc. 28 (2008) 611–616.
[48] J.E. Shelby, J.T. Kohli, J. Am. Ceram. Soc. 73 (1990) 39–42.
[49] M. Budd, Glass ceramic material and its use as means for joining different types of material and as support, Euro. Patent 0975554B1 (1998).
[50] M. Budd, Barium lanthanum silicate glass–ceramics, US Patent 7189668B2 (2007).
[51] Y.S. Chou, J.W. Stevenson, R.N. Gow, J. Power Sources 168 (2007) 426–433.
[52] Y.S. Chou, J.W. Stevenson, R.N. Gow, J. Power Sources 170 (2007) 395–400.
[53] S.T. Reis, R.K. Brow, J. Mater. Eng. Perform. 15 (2006) 410–413.
[54] R. Kirsch, Metals in Glassmaking, Glass Science and Technology, vol. 13, Elsevier, Amsterdam, 1993, chapter 9, pp. 351–355.
[55] W. Donald, J. Mater. Sci. 28 (1993) 2841–2886.
[56] M. Radovic, E. Lara-Curzio, R.M. Trejo, H. Wang, W.D. Porter, Ceram. Eng. Sci. Proc. 27 (2006) 79–85.
[57] M. Mori, Y. Hiei, N.M. Sammes, G.A. Tompsett, J. Electrochem. Soc. 147 (2000) 1295–1302.

[58] Z. Yang, Int. Mater. Rev. 53 (2008) 39–54.
[59] M. Brochu, B.D. Gauntt, R. Shah, G. Miyake, R.E. Loehman, J. Eur. Ceram. Soc. 26 (2006) 3307–3313.
[60] C. Lara, M.J. Pascual, M.O. Prado, A. Durán, Solid State Ionics 170 (2004) 201–208.
[61] R.K. Brow, H.L. McCollister, C.C. Phifer, D.E. Day, US Patent 5648302 (1997).
[62] E.S. Lim, B.S. Kim, J.H. Lee, J.J. Kim, J. Non-Cryst. Solids 352 (2006) 821–826.
[63] B.E. Yoldas, Phys. Chem. Glasses 12 (1971) 28–32.
[64] S.J. Widgeon, E.L. Corral, M.N. Spilde, R.E. Loehman, J. Am. Ceram. Soc. 92 (2009) 781–786.
[65] P. Brix, L. Gaschler, Sealing glass for the production of glass-to-metal seals, US Patent 5137849 (1992).
[66] W. Liu, X. Sun, M.A. Khaleel, J. Power Sources 185 (2008) 1193–1200.
[67] I. Avramov, J. Non-Cryst. Solids 353 (2007) 2889–2892.
[68] T. Jin, K. Lu, J. Power Sources 195 (2010) 195–203.
[69] P. McMillan, Am. Miner. 69 (1984) 622–644.
[70] B.N. Meera, J. Ramakrishna, J. Non-Cryst. Solids 159 (1993) 1–21.
[71] B.H.W.S. de Jong, C.M. Schramm, V.E. Parziale, J. Am. Chem. Soc. 106 (1984) 4396–4402.
[72] T. Maehara, T. Yano, S. Shibata, M. Yamane, Philos. Mag. 84 (2004) 3085–3099.
[73] B.H.W.S. de Jong, K.D. Keefer, G.E. Brown Jr., C.M. Taylor, Geochim. Cosmochim. Acta 45 (1981) 1291–1308.
[74] J. Deubener, J. Non-Cryst. Solids 351 (2005) 1500–1511.
[75] M.J. Hyatt, N.P. Bansal, J. Mater. Sci. 31 (1996) 172–184.
[76] P. Taylor, A.B. Campbell, D.G. Owen, J. Am. Ceram. Soc. 66 (1983) 347–351.
[77] J.H. Jean, T.H. Kuan, T.K. Gupta, J. Mater. Res. 8 (1993) 356–363.
[78] W.F. Du, K. Kuraoka, T. Akai, T. Yazawa, J. Mater. Sci. 35 (2000) 4865–4871.
[79] L.S. Du, J.F. Stebbins, J. Non-Cryst. Solids 351 (2005) 3508–3520.
[80] H. Shao, K. Liang, F. Peng, Ceram. Int. 30 (2004) 927–930.
[81] C. Lara, M.J. Pascual, R. Keding, A. Durán, J. Power Sources 157 (2006) 377–384.
[82] C. Ravagnani, R. Keding, C. Russel, J. Non-Cryst. Solids 328 (2003) 164–173.
[83] R.J. Kee, H. Zhu, A.M. Sukeshini, G.S. Jackson, Combust. Sci. Tech. 187 (2008) 1207–1244.
[84] P. Singh, S.D. Vora, Ceram. Eng. Sci. Proc. 26 (2005) 99–100.
[85] M.J. Snyder, M.G. Mesko, J.E. Shelby, J. Non-Cryst. Solids 352 (2006) 669–673.
[86] J. Simon, Ceram. Trans. 141 (2004) 389–395.
[87] T. Zhang, W.G. Fahrenholtz, S.T. Reis, R.K. Brow, J. Am. Ceram. Soc. 91 (2008) 2564–2569.
[88] V.L. Stolyarova, E.N. Plotnikov, Glass Phys. Chem. 31 (2005) 30–43.
[89] M. Tomozawa, S. Capella, J. Am. Ceram. Soc. 66 (1983) C24–C25.
[90] C.Y. Wang, L.Z. Zhou, J. Non-Cryst. Solids 80 (1986) 360–370.
[91] T.A. Wassick, R.H. Doremus, W.A. Lanford, C. Burman, Non-Cryst. Solids 54 (1983) 139–151.
[92] J. Rocherullé, F. Bourdin, R. Marchand, F. Munoz, A. Durán, Silicate Ind. 69 (2004) 113–118.
[93] J.M. Howe, Int. Mater. Rev. 38 (1993) 233–256.
[94] J.M. Howe, Int. Mater. Rev. 38 (1993) 257–271.
[95] Z. Yang, K.S. Weil, D.M. Paxton, J.W. Stevenson, J. Electrochem. Soc. 150 (2003) A1188–A1201.
[96] Z. Yang, G. Xia, K.D. Meinhardt, K.S. Weil, J.W. Stevenson, J. Mater. Eng. Perform. 13 (2004) 327–334.
[97] F. Smeacetto, M. Salvo, M. Ferraris, V. Casalegno, P. Asinari, A. Chrysanthou, J. Eur. Ceram. Soc. 28 (2008) 2521–2527.
[98] K. Ogasawara, H. Kameda, Y. Matsuzaki, T. Sakurai, T. Uehara, A. Toji, N. Sakai, K. Yamaji, T. Horita, H. Yokokawa, J. Electrochem. Soc. 154 (2007) B657–B663.
[99] K.A. Nielsen, M. Solvang, S.B.L. Nielsen, A.R. Dinesen, D. Beeaff, P.H. Larsen, J. Eur. Ceram. Soc. 27 (2007) 1817–1822.
[100] M.K. Mahapatra, K. Lu, Int. J. Appl. Ceram. Tech. 7 (2010) 10–21.
[101] M.K. Mahapatra, K. Lu, J. Mater. Sci. 44 (2009) 5369–5378.
[102] N.H. Menzler, D. Sebold, M. Zahid, S.M. Gross, T. Coppitz, J. Power Sources 152 (2005) 156–167.
[103] K.S. Weil, J.E. Deibler, J.S. Hardy, D.S. Kim, G.G. Xia, L.A. Chick, C.A. Coyle, J. Mater. Eng. Perform. 13 (2004) 316–326.
[104] C. Lara, M.J. Pascual, A. Durán, Eur. J. Glass Sci. Tech. B 48 (2007) 218–224.
[105] V.A.C. Haanappel, V. Shemet, I.C. Vinke, S.M. Gross, T.H. Koppitz, N.H. Menzler, M. Zahid, W.J. Quadakkers, J. Mater. Sci. 40 (2005) 1583–1592.
[106] P. Batfalsky, V.A.C. Haanappel, J. Malzbender, N.H. Menzler, V. Shemet, I.C. Vinke, R.W. Steinbrech, J. Power Sources 155 (2006) 128–137.
[107] A. Hauch, S.D. Ebbesen, S.H. Jensen, M. Mogensen, J. Electrohem. Soc. 155 (2008) B1184–B1193.
[108] A. Hauch, S.H. Jensen, J.B. Bilde-Sørensen, M. Mogensen, J. Electrohem. Soc. 154 (2007) A619–A626.
[109] S.P. Jiang, L. Christiansen, B. Hughan, K. Foger, J. Mater. Sci. Lett. 20 (2001) 695–697.
[110] J.H. Lee, T. Mori, J.G. Li, T. Ikegami, M. Komatsu, H. Haneda, J. Electrohem. Soc. 147 (2000) 2822–2829.
[111] K.V. Jensen, R. Wallenberg, L. Chorkendorff, M. Mogensen, Solid State Ionics 160 (2003) 27–37.
[112] Y.S. Chou, J.W. Stevenson, P. Singh, J. Power Sources 184 (2008) 238–244.
[113] Y.S. Chou, J.W. Stevenson, P. Singh, J. Power Sources 185 (2008) 1001–1008.
[114] T. Rouxel, J. Am. Ceram. Soc. 90 (2007) 3019–3039.
[115] E.V. Stephens, J.S. Vetrano, B.J. Koeppel, Y. Chou, X. Sun, M.A. Khaleel, J. Power Sources 193 (2009) 625–631.
[116] J. Malzbender, R.W. Steinbrech, L. Singheiser, J. Mater. Res. 18 (2003) 929–934.
[117] J. Malzbender, J. Mönch, R.W. Steinbrech, T. Koppitz, S.M. Gross, J. Remmel, J. Mater. Sci. 46 (2007) 6297–6301.
[118] C.K. Lin, T.T. Chen, Y.P. Chyou, L.K. Chiang, J. Power Sources 164 (2007) 238–251.
[119] K.A. Nielsen, M. Solvang, S.B.L. Nielsen, D. Beeaff, Ceram. Eng. Sci. Proc. 27 (2007) 315–323.
[120] A. Müller, S. Goswami, W. Becker, D. Stolten, L.G.J.B. de Haart, R.W. Steinbrech, Fuel Cells 6 (2006) 2107–2112.
[121] Y.S. Chou, J.W. Stevenson, L.A. Chick, J. Power Sources 112 (2002) 130–136.
[122] N. Caron, L. Blanchi, S. Methout, J. Therm. Spray Tech. 17 (2008) 598–602.
[123] T. Zhang, Q. Zhu, Z. Xie, J. Power Sources 188 (2009) 177–183.
[124] Y.L. Liu, C. Jiao, Solid State Ionics 176 (2005) 435–442.
[125] J.A. Lane, J.L. Neff, G.M. Christie, Solid State Ionics 177 (2006) 1911–1915.
[126] N. Sakai, K. Yamaji, T. Horita, Y.P. Xiong, H. Kishimoto, M.E. Brito, H. Yokokawa, Solid State Ionics 174 (2004) 103–109.
[127] S. Uhlenbruck, T. Moskalewicz, N. Jordan, H.J. Penkalla, H.P. Buchkremer, Solid State Ionics 180 (2009) 418–423.